

Gray-Scale Skeletonization of Small Vessels in Magnetic Resonance Angiography

Peter J. Yim*, Peter L. Choyke, and Ronald M. Summers, *Member, IEEE*

Abstract—Interpretation of magnetic resonance angiography (MRA) is problematic due to complexities of vascular shape and to artifacts such as the partial volume effect. We present new methods to assist in the interpretation of MRA. These include methods for detection of vessel paths and for determination of branching patterns of vascular trees. They are based on the ordered region growing (ORG) algorithm that represents the image as an acyclic graph, which can be reduced to a skeleton by specifying vessel endpoints or by a pruning process. Ambiguities in the vessel branching due to vessel overlap are effectively resolved by heuristic methods that incorporate *a priori* knowledge of bifurcation spacing. Vessel paths are detected at interactive speeds on a 500-MHz processor using vessel endpoints. These methods apply best to smaller vessels where the image intensity peaks at the center of the lumen which, for the abdominal MRA, includes vessels whose diameter is less than 1 cm.

Index Terms—Magnetic resonance angiography, skeletonization, visualization.

I. INTRODUCTION

MAGNETIC resonance angiography (MRA) is usually interpreted from the source images or from the maximum intensity projection (MIP) [1]–[4]. The MIP is useful because it is three-dimensional (3-D) in nature and thus clearly shows the overall shapes and paths of the vessels. However, the MIP reduces the contrast-to-noise ratio (CNR) of the image resulting in poor visualization of small vessels. Furthermore, the arteries may be obstructed by overlapping, high-intensity structures such as nearby veins or other arteries.

A number of methods have been developed to improve MRA visualization. One method is the use of sinc interpolation to improve the visualization of the smaller vessels in the MIP [5]. Filters have also been developed that selectively enhance vessels which make use of their tubular shape [6]–[9]. These methods are user-independent, but do not overcome problems of overlap of vessels with one another and with other anatomical structures. In this regard, the iso-intensity-surface visualization has been shown to be helpful for interpretation by providing 3-D depth cues [10]–[12] but suffers from a dependence on the selection of a single intensity threshold level. In this paper we present new gray-scale skeletonization methods for the determination of vessel paths and vessel tree structures from MRA. These methods allow for the isolation of the vasculature from

other anatomical structures and the isolation of subtrees of the vasculature from one another.

We will first discuss relevant methodologies that include segmentation and axis detection methods. We then present the ORG algorithm for skeletonization of gray-scale images. We discuss the application to abdominal MRA where the MIP may have poor quality due to high image noise, venous contamination and the presence of other high-intensity, overlapping structures. For this type of image, skeletonization requires explicit selection of the origin of the vascular tree and all vessel endpoints. We then present a method for pruning of the ORG graph to produce a skeletonization. This method requires only the specification of the topology of the vessel tree and two parameters describing the origin of the vessel tree and two parameters describing the topology of the vessel tree and is suitable for images with minimal image noise. We address the problem of determining vessel paths within dense vessel trees where nearby vessels can be mistakenly connected in the skeletonization. We present a heuristic method for preventing this type of error based on a modification of the ORG algorithm and the pruning process. Finally, we show that the skeletonization of the Circle of Willis (COW) MRA allows for a sophisticated cropping of the image to reduce the complexity of the vessel trees.

II. BACKGROUND

A variety of methods have been developed for detecting vessels within MRA. One class of methods segments or classifies voxels within the image into either vascular or nonvascular regions. The simplest segmentation method is intensity thresholding whereby points are classified as either greater or less than a given intensity. This is the basis of the iso-intensity surface reconstruction method [10]–[12]. This method suffers from errors due to image inhomogeneities and the partial volume effect. Furthermore, the choice of the threshold level is subjective.

Problems with intensity thresholding have been addressed by other segmentation methods that include the *k*-means clustering method [13], [12] fuzzy connectivity [14], the marker-controlled watershed [15] and topologically adaptive deformable models [16], [17]. These methods make use of the spatial continuity of points within the vascular tree in addition to the intensity contrast between the vessels and the surrounding tissue. However, spatial continuity is poor along narrow elongated objects such as smaller blood vessels. Thus, while these methods are adequate for segmentation of larger vessels, they commonly truncate the smaller vessels [15], [17].

An alternative to segmentation is axis detection. This is an attractive approach since vessels have a distinctively tubular shape that can be detected by the second-order partial derivatives of the image. Several methods have been developed based on this principle and multiscale schemes to allow for the diversity of vessel

Manuscript received January 26, 1999; revised April 17, 2000. The Associate Editor responsible for coordinating the review of this paper and recommending its publication was M. Sonka. Asterisk indicates the corresponding author.

*P. J. Yim, P. L. Choyke, and R. M. Summers are with the Clinical Center, NIH, Bethesda, MD 20892 USA (e-mail: pyim@nih.gov).

Publisher Item Identifier S 0278-0062(00)05731-1.

sizes [18]–[20]. However, the second derivative operations are local in nature and thus these methods require secondary operations to compose complete vessel axes. In one report, user interaction was high, presumably due to problems at bifurcations where no single direction of the vessel can be determined [18].

We propose a new method of vessel axis detection based on a single algorithm, the ORG, which encompasses both the local and global aspects of vessel detection [21]. The ORG produces a graph representation of the MRA image that describes the connectivities between all voxels in the image. From this graph, paths between any two points in the image are readily extracted. Such paths track ridges in the image intensity comparable to the marker-controlled watershed segmentation lines in two-dimensional (2-D) images [21]. Unlike similar algorithms that represent the image as an acyclic graph [22]–[24], the paths in the ORG graph have minimal dependence on seed location. The “live-wire” method, for example, will produce paths that have the least cumulative “cost” which is a function of the path length and image intensities along the path. As such, highly curved paths are discouraged and the method is only reliable in the vicinity of the seed point.

The ORG algorithm is defined as follows. As shown in Fig. 1, the ORG is an iterative region-growing process whereby at any given iteration, growth occurs from the point on the boundary of the grown region with the highest image intensity. For an N -dimensional image $I: \mathbf{Z}^N \rightarrow \mathbf{Z}$, let R_n represent the voxels within the region at iteration n . Let B_n be the boundary of R_n . At each iteration, $B_n \subseteq R_n$. R_0 is any point or points in the image which is the *seed region* which is specified by the user. B_0 is the boundary of that region. G_n is then the set of growth points at the n th iteration. $\text{Neighbor}(\cdot)$ refers to the set of immediate neighbors of a single point, either 8 or 26-neighbor for the 3-D case, (26-neighbor is used here), and $\text{Max}(\cdot)$ refers to the point of maximum intensity of a set of points. If more than one point in B_n shares the maximum intensity value, $\text{Max}(\cdot)$ is arbitrarily chosen from amongst those points. If the intensity range within the image is large, this ambiguity is of minor importance.

$$s_n = \text{Max}(B_n) = \{x \in B_n | \forall y \in B_n, I(x) \geq I(y)\} \quad (1a)$$

$$G_n = \text{Neighbor}(s_n) \setminus R_n \quad (1b)$$

$$B_{n+1} = (B_n \cup G_n) \setminus s_n \quad (1c)$$

$$R_{n+1} = R_n \cup G_n. \quad (1d)$$

Certain advantages may be gained by the selection of meaningful seed points such as those at the origin of a vascular tree of interest so as to establish the correct *directionality* of the skeleton although the *connectivity*, is largely independent of the seed-point placement with small-scale variability occurring in the vicinity of bifurcations [21].

Connections or edges E can be described by the pair of points which they connect

$$E_{n+1} = E_n \cup \{(s_n, g_n) | g_n \in G_n\} \quad (2a)$$

$$E_0 = \emptyset. \quad (2b)$$

The directionality, which may be meaningful by itself, can be expressed as a mapping from a given point to its parent $P: \mathbf{Z}^N \rightarrow \mathbf{Z}^N$

$$P(g_n) = s_n \quad (g_n \in G_n). \quad (3)$$

The ORG graph of a synthetic 2-D image is shown in Fig. 2.

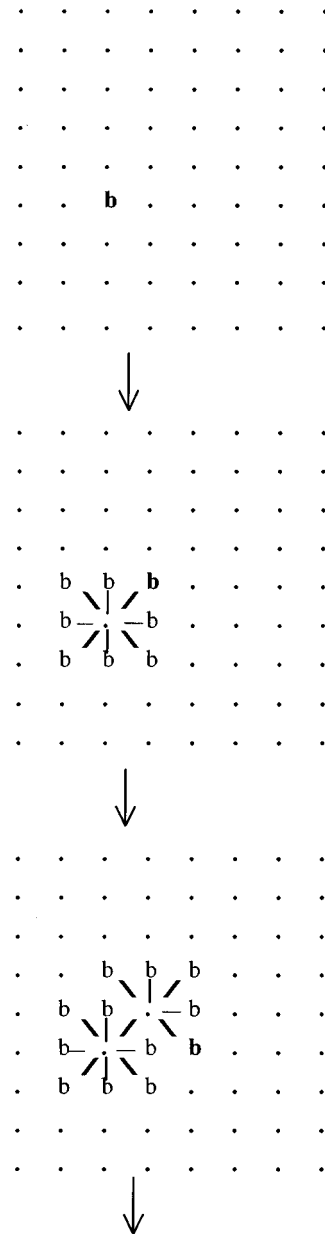


Fig. 1. Two-dimensional example of ORG connectivity algorithm. Region grows to neighboring points from a user-specified seed point (b in top diagram). The seed point for succeeding iterations are the points of maximum intensity of the region boundary ($b = s_n$). The direction of the growth (shown by hash marks) is recorded at each iteration and cumulatively forms a graph representation of the image. The points b are the elements of the boundary region B_n .

III. SKELETONIZATION BY EXPLICIT SELECTION

A. Algorithm

Skeletonization of a given vessel tree can be performed by explicitly selecting the origin of the vessel tree and the endpoints of the vessels. The origin of the vessel tree serves as the seed point of the ORG graph. Vessel paths are determined by simply retracing the path from each endpoint to the ORG origin.

The skeletal paths are defined precisely as follows. For all points i within an image I , a skeleton S can then be defined as all those points from which the set of user-defined endpoints

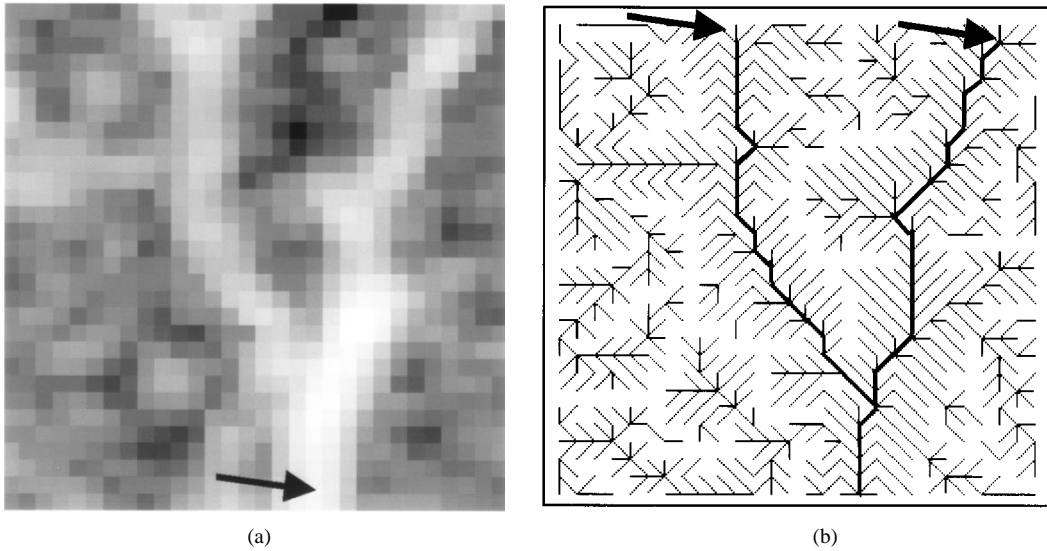


Fig. 2. ORG applied to a low-resolution 2-D image (left) originating at the point indicated by the arrow. The ORG acyclic graph is shown at right (directionality of graph is not shown). A significant path is determined from this connectivity structure and the indication of additional points (arrows on right). In this way, centerlines of the vessels in the MRA can be detected by the indication of a single seed point at the proximal end of a vascular tree and points at the distal ends of all terminal vessel segments.

EP 's are descended as well as those peripheral points themselves with the connectivity of these points determined by the ORG algorithm. The set, $\text{Descendents}(i)$, are all points which are descended from the point i in the course of the ORG growth. More formally, the descendents of i are all the points which are disconnected from the rest of the graph if that point and its associated connections are removed.

A Path (a, b) is the set of points traversed going from a to b along the ORG graph, including a and b . This can be expressed as follows:

$$\text{Descendents}(i) = \{d \in I | i \in \text{Path}(d, P(i)), d \neq i\}. \quad (4)$$

Then

$$S = \{i \in I | \text{Descendents}(i) \cap EP \neq \emptyset\} \cup EP. \quad (5)$$

To avoid the larger vessels such as the aorta where the ORG skeletonization does not apply, multiple seed points must be provided. For application to hepatic MRA, seed points are placed at the origin of the celiac trunk and the superior mesenteric artery which are two of the major vessels in the abdomen. In this case, no relevant vessel paths pass through the aorta.

Once the ORG graph is constructed, the vessel paths are determined in real-time for each vessel endpoint selected. Errors in skeletonization occur if the selected point is not directly on the vessel or if the segment of the vessel is too faint to be detected by the ORG algorithm. In the latter case, the point must be reselected at a more proximal point along the vessel from which a more distinct path exists to the origin of the ORG.

B. Application

Angiography is essential for preoperative planning prior to hepatic perfusion for tumor therapy and prior to liver transplantation. MRA has become a viable and less invasive

approach than conventional digital subtraction angiography [25], [26]. The ORG skeletonization can be used to highlight relevant vessel paths within the image as shown in Fig. 3. This method has been found to accurately portray the vascular paths and to be useful for 3-D visualization of the vascular anatomy [27]. Typically, distal points are identified on the source images where the small vessels are most visible from which the complete path back to the origin of the vessel tree is determined and displayed in a 3-D form.

IV. SKELETONIZATION BY PRUNING

A. Algorithm

A second method of skeletonization is one that requires the operator only to supply the seed point and two parameters that describe the desired topology of the vessel tree. This method is based on a pruning process in which trivial branches are removed from the ORG graph, while true vessel axes are retained. We propose a pruning process based upon branch length. In this pruning process, branches are discarded if they do not have a given minimal length. The concept of pruning by branch length is shown in Fig. 4.

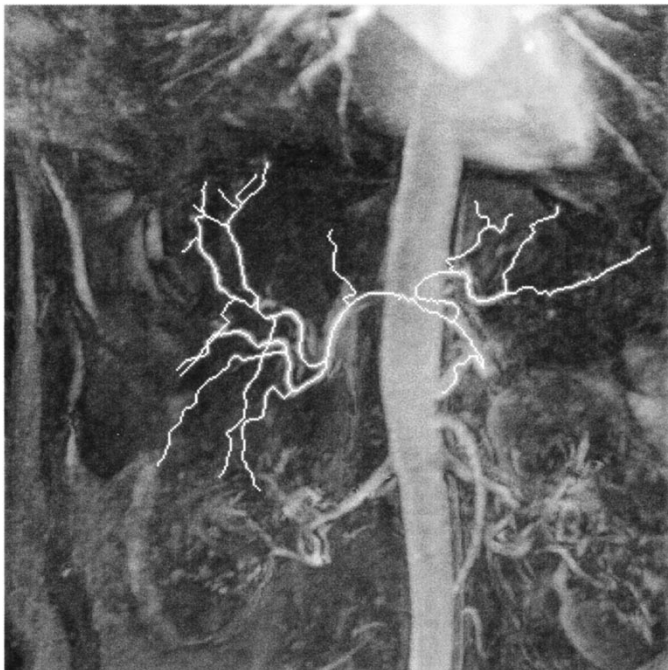
The specific pruning criteria is that no branch is retained if the distance from the terminus to the nearest bifurcation is less than a given minimum length. This result is obtained as follows. Let R be the region overgrown by the ORG in which the intensity of all points in the region are greater than some given threshold value. Let $\text{Siblings}(i)$ be the set of all points with a common ORG parent:

$$\text{Sibling}(i) = \{j \in R | P(j) = P(i), i \neq j\}. \quad (6)$$

Let L be the connectivity distance from a given point i to its furthest descendent within the ORG. This is effectively, the branch length of the point i . The distance, $D: \mathbf{Z}^N \times \mathbf{Z}^N \rightarrow \mathbf{Z}$, is just the number of connections between any two points within



(a)



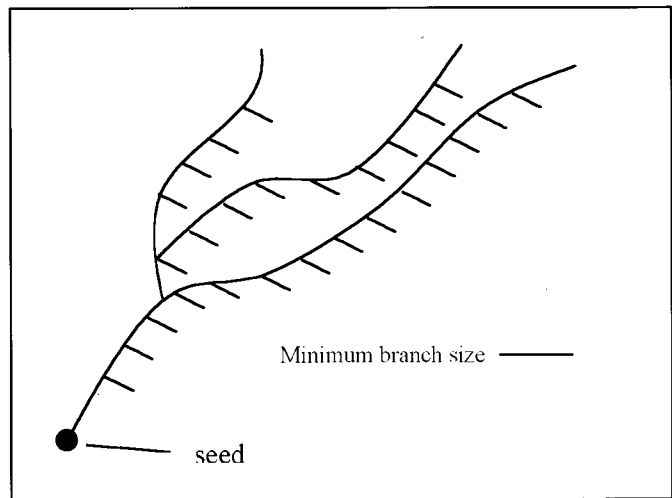
(b)

Fig. 3. Clarification of anatomy of hepatic circulation. The MIP view of the original image is shown at the top. The image on the bottom shows the skeletonization produced by explicit specification of endpoints superimposed on the MIP showing the paths of the smaller vessels with greater clarity. In this case, all distal endpoints of the vessels are identified by the user while the corresponding skeletal paths are determined and displayed in real-time. These endpoints may identified either in individual slices or in MIP views. Determination and documentation of vascular anatomy of the liver is important for surgical planning.

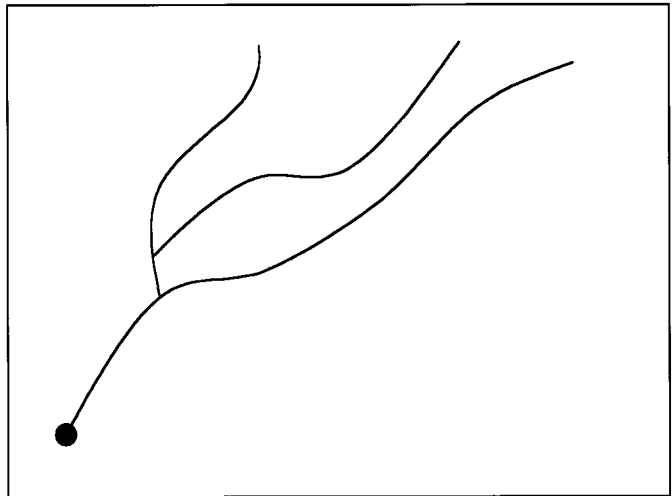
the connectivity graph. (This definition can also apply to two given *edges* in the graph.)

$$L(i): Z^N \rightarrow Z \text{ defined as}$$

$$L(i) = \text{Maximum}(\{D(d,i) | d \in \text{Descendants}(i)\}), \quad (7)$$



(a)



(b)

Fig. 4. Skeletonization by pruning. A connectivity tree, such as (a) is produced by the ORG, can be reduced to its (b) most essential components by rejecting branches whose length is less than some given minimum, as is described in more detail in the text.

MIN is the minimum branch length that qualifies for a bifurcation; one parameter of the skeletonization. Then S is the set of points constituting the pruned skeleton

$$T = \{i \in R | L(i) < \text{MIN} - 1\}$$

$$\cap \{i \in R | \exists k \in \text{Siblings}(i), L(i) < L(k)\} \quad (8a)$$

$$D = \{\text{Descendants}(t) | t \in T\} \cup T \quad (8b)$$

$$S = R \setminus D. \quad (8c)$$

The pruning process can be performed efficiently as follows:

- 1) Compute ORG connectivity of given region R from seed point;
- 2) Initialize branch lengths $L(i)$ of all points to 0;
- 3) Until reach steady state (no further changes in values of L for any point): for all i in R if $L(i) > L(P(i)) - 1$ then $L(P(i)) = L(i) + 1$;
- 4) Initialize all points in a "skeleton" image, Skeleton, to 1;

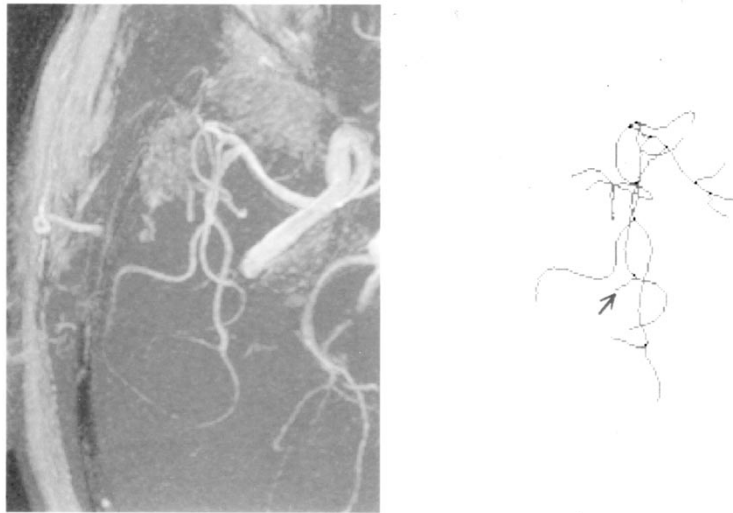


Fig. 5. Skeletonization by pruning. Region of cerebral vasculature (middle cerebral artery tree) was skeletonized by pruning process. MIP of region of original image is shown at left and 2-D projection of skeletonization is shown at right. Bifurcation points are indicated as the darker points. Direction of flow of the vessels, not shown in this visualization, is also obtained from the skeletonization process. This skeletonization requires only the identification of a single seed point at a proximal location on the vascular tree and the nulling of the vessel in the upstream direction along with the specification of the desired number of bifurcations and minimum branch length. In this particular case, only one connectivity error was found in this result as indicated by the arrow. Due to the conservative nature of the region growing for the purposes of this study, some segments of vessels visible in the MIP are not represented in the skeletonization.

- 5) For all i in R :
 - for all j siblings of point i ;
 - if $L(i) < L(j)$ and $L(i) < \text{Min}$;
 - then $\text{Skeleton}(i) = 0$;
- 6) Until reach a steady state (no further changes in any Skeleton) for all i in R ;
- if $(\text{Skeleton}(\text{Parent}(i)) = 0)$;
- $\text{Skeleton}(i) = 0$.

The ORG growth can be constrained by a specified number of bifurcations as opposed to a given threshold intensity value. This method reduces the dependence of the skeletonization on absolute image intensity values. This can be carried out efficiently by updating the number of qualifying bifurcations in the course of the ORG growth.

B. Application to Circle of Willis (COW) MRA

The pruning skeletonization process applies best to low-noise images with minimal inhomogeneities. Such conditions exist for the COW MRA. The skeletonization was tested on three images of the COW vasculature obtained with a standard MRA Spoiled Gradient Recalled Echo, time of flight sequence. (Flow compensated, magnetization transfer background suppression, superior flow saturation, 25° flip angle, 1.4-mm-thick slices, 35 ms TR, minimum TE, 256×224 matrix, 1 excitation.) Three regions were skeletonized in each image including the vessel tree downstream from the basilar artery and from the right and left middle cerebral arteries (MCA's). The minimum branch length was set to 15 and 25 voxel units the number of bifurcations was 5 and 10. (The length of a branch was considered to be the number of voxels within the branch). Each combination of the two parameters was tested. A region immediately upstream of each seed point was nulled to prevent upstream growth of the ORG algorithm. An example of a result of skeletonization of the COW is shown in Fig. 5.

TABLE I
PERFORMANCE OF BASIC SKELETONIZATION-BY-PRUNING ALGORITHM ON CEREBRAL MRA. ALGORITHM APPLIED TO MIDDLE CEREBRAL ARTERIES (MCA) AND BASILAR ARTERY IN THREE MRA'S. NUMBERS IN PARENTHESIS IN "STUDY CONDITION" COLUMN REFER TO SPECIFIED NUMBER OF BIFURCATIONS AND MINIMUM BRANCH LENGTH (IN VOXEL UNITS) RESPECTIVELY. THE SAMPLES WERE TAKEN FROM THREE SUBJECTS WITH TWO MCA AND ONE BASILAR ARTERY TREES FROM EACH SUBJECT

Study Conditions	Number of Samples	Connectivity Errors (average)
MCA (5,15)	6	2.3±1.5
MCA (10,15)	6	3.0±1.7
MCA (5,25)	6	2.1±1.5
MCA (10,25)	6	3.5±1.4
basilar (5,15)	3	0.0±0.0
basilar (10,15)	3	1.0±1.7
basilar (5,25)	3	0.0±0.0
basilar (10,25)	3	2.0±1.7

Each vessel segment within the skeleton was rated as correct if the origin of the segment was attached to the correct upstream vessel segment. The region overgrown by the ORG was nearly always completely within the region of the vessels and thus nearly all branches in the skeletonization corresponded to vessel branches. The results of the skeletonization are shown in Table I. In a cropped $100 \times 200 \times 100$ region of the image that encompasses all visible vessels downstream of the MCA, the entire skeletonization computation requires less than 10 s on the MIPS 10 000 195-MHz processor.

One error in all of the skeletonizations was due to a leakage of the skeleton into a nonvascular region, all other errors were due to incorrect connectivity of vessels. The connectivity errors occurred where significant overlap of image intensity occurred between nearby vessels. A greater number of errors occurred in the arteries descended from the MCA than from the basilar artery due to a greater apparent density of vessels descended from the

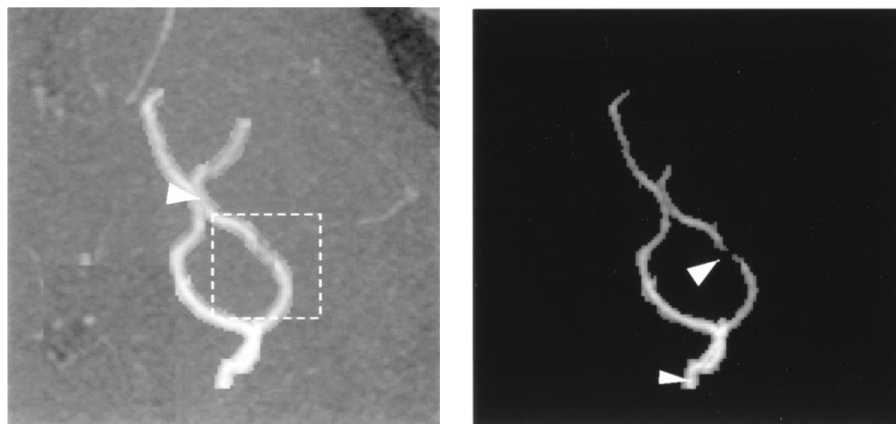


Fig. 6. Effect of vessel overlap on ORG process. A 2-D test image simulates the effect of distinct vessels appearing to overlap one another due to their close proximity (arrowhead at left). The right image shows the region overgrown by the ORG (originated at small arrowhead) at one given point in the process. In this case, the ORG incorrectly connects the vessels at the overlap point and breaks the connectivity within a vessel (large arrowhead on right). However, these break points are usually relatively obvious and can be mended as is discussed in following sections. Note also that within a subregion of the image (dotted square on right) the ORG would produce the correct connectivity along the vessel.

MCA. For a minimum branch length of 15, and for vessel trees with ten bifurcations, there were an average of 3.0 ± 1.7 errors in the MCA regions and 1.0 ± 1.7 errors in the basilar artery regions. These connectivity errors are most common amongst the largest vessels which are present in both skeletons with five and with ten bifurcations. Thus the rate of this type of error does not increase proportionally as the specified number of bifurcations increases. For example, for the MCA region with a minimum branch length of 15 voxel units, there are 2.3 ± 1.5 errors for skeletons with five bifurcations compared to 3.0 ± 1.7 errors for skeletons with ten bifurcations.

V. THE PROBLEM OF VESSEL OVERLAP

A. Modification of the ORG Algorithm

The acyclic topology of the ORG graph is quite appropriate for analysis of vascular trees that are themselves nearly acyclic in nature. However, this model has limitations when applied to *images* of vessel trees where apparent loops occur when vessels are highly overlapped. While, in some cases, the ORG algorithm can successfully separate the distinct vessels from one another, it is susceptible to error. This is the source of nearly all the errors described in the previous section. Apparent loops in the vessel tree result in the incorrect joining of distinct vessels. Since no loops can exist in the graph, for each such error, a second error will occur in which a vessel segment is disjointed from itself.

A step toward resolving this problem is to allow for a limited number of cycles to be included in the graph. Pruning of this graph would then be similar to before. However, in this case, additional methods would be necessary to correctly reduce cycles in the graph to the correct acyclic form which correctly depicts the branching structure of the vessels.

The desired graph which allows for a limited number of cycles can be obtained by a minor modifications of the ORG algorithm. This is clear from the following observation: At points where vessels are incorrectly disjointed in the ORG graph, continuity is usually obvious at the local level or within a cropped subregion of the image. If, for example, the ORG algorithm were only applied to the subregion, the ORG would form an

uninterrupted path along the vessel axis. Thus, the local ORG graph contains the desired connections which are missing from the global ORG graph. An automated scheme, which is derived from that observation, is difficult to imaging since it requires the selection of the size and location of the cropped region. However, another approach will produce similar results. In this approach, growth occurs according to (1a)–(1d) except that connections are formed between points of two different growth fronts that collide with one another. An example of such a collision is illustrated in Fig. 6. In effect, cycles are formed in the ORG graph provided they are of sufficient circumferential size.

The path along a vessel axis to either side of the collision is the same as that which would be produced by a local ORG growth that proceeds in a single direction along the vessel axis. This is true because ORG paths are independent of the direction of the ORG growth that formed the path [21].

B. Implementation of a Modified ORG Algorithm

The modified ORG algorithm described in the previous section can be implemented in an efficient manner using the assumption that significant collisions that disjoint vessel segments are uncommon and occur in isolation from one another. Under that assumption, the size of a cycle formed in a collision can be determined simply by looking upstream from each collision point until the common branch point is encountered. In this case where the search only includes upstream points, circumferential length can be determined quickly.

The modification to the connectivity of the basic ORG [from (2)] is described below. A set of new edges E' is added to the set of edges E of the basic ORG. The qualifications for the edges in E' are described in (9a). Any cycle in the ORG graph must have a circumferential size greater than some minimum value CS_{\min} . Furthermore, to enforce the assumption that cycles in the graph occur in relative isolation from one another, all the cyclic edges in E' are required to be a distance of CS_{\min} from one another.

Let (a, s_n) be an edge which connects the growth point s_n at any iteration to one of its neighbors a , which is already in the grown region R , $(a \in \text{Neighbor}(s_n) \setminus G_n)$ [G_n defined in (1b)]. Let $CS_n: \mathcal{Z}^N \times \mathcal{Z}^N \rightarrow \mathcal{Z}$ be a function which determines, for

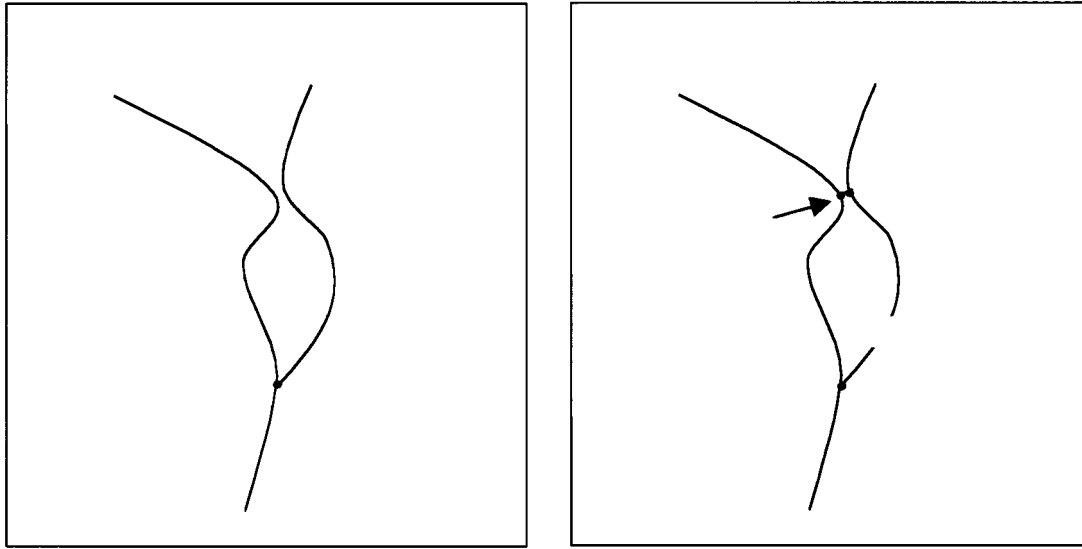


Fig. 7. Detection of incorrect skeletonization. Under conditions where two vessels nearly intersect skeletonization based on the basic ORG may incorrectly connect the two vessels at that point. Thus, rather than producing the correct connections of the vessel, a trifurcation-like structure may be formed in the skeleton consisting of two nearby bifurcations (two dark dots indicated by arrow at right). The existence of such trifurcations can generally be distinguished from normal anatomy and thus such errors in the skeletonization can be corrected, as described in the text.

any given edge added to the ORG connectivity at a given iteration, what the size of the minimum-sized cycle it is associated with. *Arbitrary()* is a function that arbitrarily chooses one element of a set which in this case is determined by the scan order at each iteration.

$$E_{\text{pot},n} = \{a - s_n \mid \text{CS}_n(a, s_n) > \text{CS}_{\text{min}}\} \\ \cap \{a - s_n \mid \forall e' \in E'_n, D(e', a, s_n) > \text{CS}_{\text{min}}\} \quad (9a)$$

$$E'_{n+1} = E'_n \cup \{\text{Arbitrary}(E_{\text{pot},n}) \mid E_{\text{pot},n} \neq \emptyset\} \quad (9b)$$

$$E_{n+1} = E_n \cup \{(g, s_n) \mid g \in G_n\} \cup E'_{n+1}. \quad (9c)$$

C. Modified Skeletonization by Pruning

The results of the basic skeletonization by pruning method (Section IV) can be improved using the modified ORG. The method for extending the skeletonization by pruning is heuristic and is based on the observation that, within the higher order branchings of the vasculature, bifurcations do not occur in close proximity to one another. Even in so-called trifurcations such as in the popliteal artery, there is substantial separation between two distinct bifurcations. This observation is relevant to skeletonization since apparent trifurcations tend to be produced when two distinct vessels nearly intersect and are incorrectly joined in the skeleton. This situation is illustrated in Fig. 7. The method we propose removes trifurcation-like formations in the skeletonization.

First, the modified ORG graph is pruned as described in Section IV without regard for edges specific to the modified ORG except that branches upstream from collisions are not pruned. Then all possible alternative acyclic skeletonizations are formed by the inclusion of one or more of the cyclic edges produced by the modified ORG and a corresponding removal of one of the original edges. For each of these alternative skeletonizations, the one in which all the bifurcations have the greatest degree of separation from one another is preferred.

Stepwise the algorithm proceeds as follows:

1. *Apply modified ORG algorithm.*
2. *Determine the basic skeletonization by pruning (Section IV).*
3. *Determine if the basic skeletonization by pruning can be improved, in terms of reducing any “trifurcations,” by the inclusion of one or more of the “reconnection” edges from the modified ORG. For each “reconnection” edge: a. Add points to basic skeleton so as to complete the cycle associated with the reconnection edge. For purposes of evaluating trifurcations, trim off any trivial branches produced by this step (less than 5 voxel units long). b. Determine the most likely trifurcation point within the cycle (where the skeleton literally divides in three or where there are two bifurcations in close succession). Then, remove the trifurcation: If the trifurcation is composed of two bifurcations which are both within the cycle, simply remove the segment of the skeleton between the two bifurcations so as to obtain an acyclic skeleton. Otherwise, consider the trifurcation to be detected-but-not-corrected. In that case, arbitrarily remove an edge in the skeleton adjacent to the trifurcation which is within the cycle so as to obtain an acyclic skeleton.*

Performance of the Modified Skeletonization by Pruning algorithm was evaluated and compared with that of the basic Skeletonization by Pruning. For these tests, a slight difference in the implementation of the Modified ORG from that described in (9) was used in which the distance between any two cyclic edges in E' was considered to be the maximum of the distance from either of the two points to their mutual bifurcation point in the ORG graph as opposed to the sum of the distance from each of the two points to their mutual bifurcation point. The cycle size, CS, was determined in a similar way. This difference in implementation, we believe, is unlikely to produce results significantly different from those that would be produced by a

TABLE II
COMPARISON OF MODIFIED SKELETONIZATION BY PRUNING ALGORITHM WITH THE BASIC SKELETONIZATION BY PRUNING ALGORITHM (ALGORITHM 2). REFER TO TABLE I FOR EXPLANATION OF "STUDY CONDITIONS"

Study Conditions	Number of Samples	Added Connections (average)	Correctly Added Connections (average)	Remaining Missing Connections (average)
MCA (5,15)	6	1.0±0.6	0.5±0.5	0.3±0.8
MCA (10,15)	6	3.2±1.6	1.0±0.8	0.2±0.4
MCA (5,25)	6	1.5±0.5	0.8±0.7	0.2±0.4
MCA (10,25)	6	3.5±1.0	1.2±0.9	0.2±0.4

TABLE III
ERRORS IN CONNECTIVITY AFTER APPLICATION OF TRIFURCATION REDUCTION ALGORITHM IN MCA ARTERY WHERE THERE IS GREATEST DEGREE OF VESSEL OVERLAP

Study Conditions	Number of Samples	Undetected Connectivity Errors (average)	Detected but Uncorrected Errors (average)
MCA (5,15)	6	0.8±1.2	0.2±0.2
MCA (10,15)	6	0.3±0.8	0.2±0.2
MCA (5,25)	6	0.7±1.1	0.3±0.3
MCA (10,25)	6	0.7±1.1	0.2±0.2

direct implementation of the algorithm described by (9). For these tests, the minimum cycle size, CS_{\min} was set to be the same as that of the minimum branch length.

The results were assessed only in the MCA artery region where there were a sizeable number connectivity and directionality errors in pruning of the basic ORG. The net result of the modified skeletonization by pruning was that less than 1 connectivity error occurred within the vessels skeletonized under all conditions as is shown in Table III. The complete computation of the skeleton, after the interactive initialization of the algorithm, took less than 10 s on $100 \times 200 \times 100$ region.

VI. ARTERY-ARTERY SEPARATION

The high density and overlapping nature of the cerebral vascular tree makes visualization of individual vessels in MIP projections difficult, particularly when vessels are highly enhanced by high flow rates [28] even with careful selection of the MIP orientation and slice range. This problem has been addressed by the application of shaded surface display to provide depth information [1] and by a method whereby both the surface and medial axes are detected allowing for selective colorization [29]. In a likewise, but more powerful way, the cerebral skeletonization can be used to improve the quality of the visualization. The method suggested here is to effectively disentangle or separate the arterial subtrees. Given that centerlines of vessels can be identified reliably by the methods described in the previous sections specific vascular subtrees can easily be identified, based on, for example, the specification of the origin a particular vessel. Points nearby to the skeleton downstream of the indicated point are set to zero intensity. Specifically, good results have been found zeroing out points within two 26-neighbor dilation iterations of the downstream skeleton. The result of the application to a cerebral

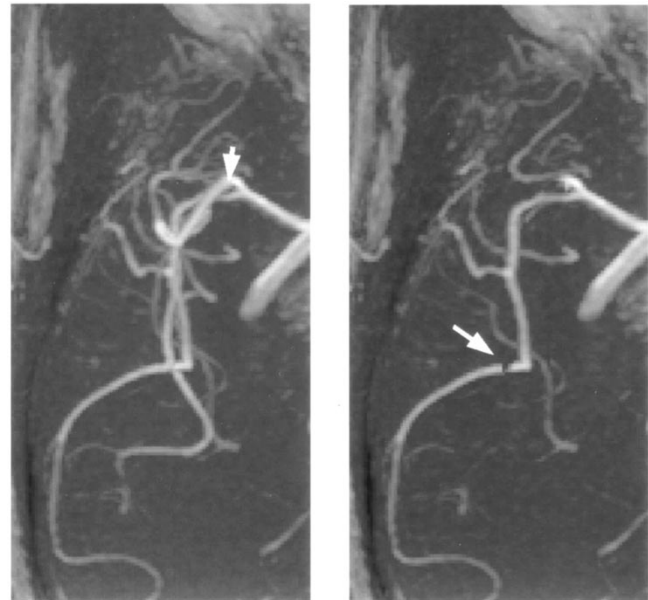


Fig. 8. Artery-artery separation. The portion of the vascular tree downstream of a given point on the vascular tree (arrow on left image) is nulled according to the connectivity of the Modified ORG Skeletonization within 2 iterations of a 27-neighbor dilations. Note a small section of an artery has been unintentionally nulled (arrow in right image) due to the close proximity of distinct vessels. This method is useful for obtaining an unobstructed view of individual vessels in the cerebral MRA.

vascular tree is shown in Fig. 8. Once the desired skeleton of the vascular tree has been produced, this disentangling procedure can be conducted in a very interactive manner; the nonoptimized speed is less than 5 s on a $100 \times 200 \times 100$ cropped region.

VII. CONCLUSION

In this paper we address the problems of visualization and characterization of small vessels in MRA which are inadequately resolved by other methods. These problems include that of detection of the paths of smaller vessels under conditions where regional or intensity-based segmentation methods are inadequate in the abdominal MRA and the problem of determination of the proper connectivity or anatomical relations of the vessels such as in the cerebral MRA. Like several other methods [18]–[20] these problems are addressed within the framework of gray-scale operations, but the new principle of ORG connectivity applied to this problem incorporates global gray-scale intensity properties and topological constraints into

the formation of the centerlines both of which are absent from previous methods. Specifically, paths are formed according to the greatest-minima property such that they follow the center of the vessels, to within the resolution of the image grid, provided that the image intensity of the vessels peak toward their center, which is typical for smaller vessels in MRA.

In implementation, the methods are practical and fast. All the methods are interactive in nature but small-scale variations in user input have relatively minor effect on the resulting path determinations. Methods presented for the *detection* of vessels using ORG connectivity in the abdominal MRA or in the smaller vessels of the cerebral MRA are the most intensely interactive requiring the specification of all distal endpoints. Improvement in the automation of this method within the context of the ORG is entirely possible and will be the subject of future work. We also believe that the paths may be incorporated into improved methods for determination of vessel diameter and will be the subject of future work.

REFERENCES

- [1] D. B. S. Johnson, M. R. Prince, and T. L. Chenevert, "Magnetic resonance angiography: A review," *Acad. Radiol.*, vol. 5, pp. 289–305, Apr. 1998.
- [2] B. Siewert, M. R. Patel, and S. Warach, "Magnetic resonance angiography," *Neurologist*, vol. 1, pp. 167–184, May 1995.
- [3] J. F. Debatin and T. F. Hany, "MR-based assessment of vascular morphology and function," *Eur. Radiol.*, vol. 8, pp. 528–539, 1998.
- [4] S. Rossnick, G. Laub, and R. Braeckle *et al.*, "Three dimensional display of blood vessels in MRI," in *Proc. IEEE Comput. Cardiol. Conf.*, 1986, pp. 193–196.
- [5] Y. P. Du, D. L. Parker, W. L. Davis, and G. Cao, "Reduction of partial-volume artifacts with zero-filled interpolation in three-dimensional MR angiography," *J. Magn. Reson. Imag.*, vol. 4, pp. 733–741, 1994.
- [6] Y. P. Du, D. L. Parker, and W. L. Davis, "Vessel enhancement filtering in three-dimensional MR angiography," *J. Magn. Reson. Imag.*, vol. 5, pp. 353–359, 1995.
- [7] W. Lin, E. M. Haacke, T. J. Masaryk, and A. S. Smith, "Automated local maximum-intensity projection with three-dimensional vessel tracking," *J. Magn. Reson. Imag.*, vol. 2, pp. 519–526, 1992.
- [8] M. M. Orkisz, C. Bresson, I. E. Magnin, O. Champin, and P. C. Douek, "Improved vessel visualization in MR angiography by nonlinear anisotropic filtering," *Magn. Reson. Imag.*, vol. 37, pp. 914–919, 1997.
- [9] H. Chen and J. Hale, "An algorithm for MR angiography image enhancement," *Magn. Reson. Imag.*, vol. 33, pp. 534–540, 1995.
- [10] H. E. Cline, W. E. Lorensen, R. Kikinis, and R. Jolesz, "Three-dimensional segmentation of MR images of the head using probability and connectivity," *Neurosurgery*, vol. 14, pp. 1037–1045, 1990.
- [11] S. Nakajima, H. Atsumi, and A. H. Bhalerao, *et al.*, "Computer-assisted surgical planning for cerebrovascular neurosurgery," *Neurosurgery*, vol. 41, pp. 403–409, 1997.
- [12] H. E. Cline, W. E. Lorensen, S. P. Souza, F. A. Jolesz, R. Kikinis, G. Gerig, and T. E. Kennedy, "3D surface rendered MR images of the brain and its vasculature," *JCAT*, vol. 15, pp. 344–351, 1991.
- [13] D. L. Wilson and J. A. Noble, "Segmentation of cerebral vessels and aneurysms from MR angiography data," vol. 1230, 1997. *Lecture Notes in Computer Science*.
- [14] T. Lei, J. K. Udupa, P. K. Saha, and D. Odhner, "MR angiographic visualization and artery-vein separation," *Proc. SPIE*, vol. 3658, pp. 58–66, 1999.
- [15] P. J. Yim, D. Kim, and C. Lucas, "High resolution four-dimensional surface reconstruction of the right heart and pulmonary arteries," *Proc. SPIE*, vol. 3338, pp. 726–738, 1998.
- [16] T. McInerney and D. Terzopoulos, "Deformable models in medical image analysis: A survey," *Med. Image Anal.*, vol. 1, pp. 91–108, 1996.
- [17] A. J. Bulpitt and E. Berry, "Spiral CT of abdominal aortic aneurysms: Comparison of segmentation with and automatic 3D deformable model and interactive segmentation," *Proc. SPIE*, vol. 3338, pp. 938–946, 1998.
- [18] S. Aylward, E. Bullit, S. Pizer, and D. Eberly, "Intensity ridge and widths for tubular object segmentation and description," *Proc. IEEE Wkshp.*, June 1996. *Math. Meth. Biomed. Image Anal.*
- [19] Y. Sato, S. Nakajima, H. Atsumi, T. Koller, G. Gerig, S. Yoshida, and R. Kikinis, "3D multi-scale line filter for segmentation and visualization of curvilinear structures in medical images," *Lecture Notes in Comput. Sci.*, vol. 1205, pp. 213–222, 1997.
- [20] C. Lorenz, I.-C. Carlsen, T. M. Buzug, C. Fassnacht, and J. Weese, "Multi-scale line segmentation with automatic estimation of width, contrast, and tangential direction in 2D and 3D medical images," *Lecture Notes in Comput. Sci.*, vol. 1205, pp. 233–242, 1997.
- [21] P. J. Yim, D. Kim, and R. M. Summers, "A path-wise definition of the watershed line and a watershed-like skeletonization", submitted for publication.
- [22] E. W. Dijkstra, "A note on two problems in connexion with graphs," *Numerische Mathematik*, vol. 1, pp. 269–271, 1959.
- [23] A. X. Falco, J. K. Udupa, S. Sanaraskeras, S. Shoba, B. E. Hirsch, and R. A. Lotufo, "User-steered image segmentation paradigms: Live wire and live lane," *Proc. SPIE*, vol. 2710, p. 278, 1996.
- [24] J. R. Lersch, A. E. Iverson, B. N. Webb, and K. F. West, "Segmentation of multiband imagery using minimum spanning trees," *Proc. SPIE*, vol. 2758, pp. 10–18, 1996.
- [25] P. Choyke and B. Damaska, "Gadolinium enhanced 3-D TOF MRA in the preoperative mapping of hepatic arteries prior to isolated perfusion therapy of metastatic disease of the liver," in *Proc. 6th Annu. Meeting. ISMRM*, 1998, p. 222.
- [26] H. Zeh, P. L. Choyke, H. R. Alexander, D. L. Bartlett, S. K. Litutti, R. Chang, and R. M. Summers, "Gadolinium enhanced 3-D magnetic resonance angiography prior to isolated hepatic perfusion for metastases," *JCAT*, vol. 23, pp. 664–669, Sept.–Oct. 1999.
- [27] P. L. Choyke, P. J. Yim, H. Marcos, V. B. Ho, R. Mullick, and R. M. Summers, "Hepatic magnetic resonance angiograms: A multiobserver comparison of visualization methods," *AJR*, submitted for publication.
- [28] A. R. Gilliams, L. McMahan, G. Wernberg, and A. P. Carter, "MRA of the intracranial circulation in asymptomatic patients with sickle cell disease," *Pediat. Radiol.*, vol. 28, pp. 283–287, 1998.
- [29] E. Bullit, A. Liu, S. Aylward, M. Soltys, J. Rosenman, and S. M. Pizer, "Methods for displaying intracerebral vascular anatomy," *AJNR*, vol. 18, pp. 417–420, Mar. 1997.